Measurement quality of a software defined radio system for medical diagnostics

Received: 20 May 2022 | Revised: 25 August 2022 | Accepted: 4 September 2022

DOI: 10.1049/tje2.12196

The Journal of Engineering

The Institution of Engineering and Technology WILEY

ORIGINAL RESEARCH

Measurement quality of a software defined radio system for medical diagnostics

Xuezhi Zeng | **Laura Guerrero Orozco**

Biomedical Electromagnetics Research Group, Department of Electrical Engineering, Chalmers University of Technology, Gothenburg, Sweden

Correspondence
Xuezhi Zeng, Biomedical Electromagnetics Research Group, Department of Electrical Engineering, Chalmers University of Technology, SE 412 58, Gothenburg, Sweden.
Email: xuezhi@chalmers.se

Funding information
VINNOVA

Abstract

The measurement quality of a software defined radio system was investigated and discussed for medical diagnostics in the frequency band of interest 500 MHz–2 GHz. A calibration approach was proposed in order to deal with the random phase problem, and the obtained performance was evaluated and benchmarked against a vector network analyser. The results suggest that the measurement quality of the software defined radio system is mainly limited by the signal leakage from the transmitter to the receiver. Good agreement between the measurement data obtained with the software defined ratio system and the network analyser was achieved when the transmission loss is less than 70 dB. With some a priori knowledge of the measured object, the software defined radio system is able to perform accurate measurement when the transmission loss is even higher.

1 | INTRODUCTION

Over the past years, microwave technology has been broadly explored for various medical applications, such as disease detection and tumour treatment [1]. Particularly, microwave based diagnostics of stroke and trauma has received considerable attention as this novel diagnostic tool could be brought to the point of care, enabling prehospital diagnosis, which could largely reduce mortality and societal cost [2].

The possibility of using microwave-based technology for medical diagnostics relies on the existence of a contrast in the dielectric parameters between healthy tissues and diseased tissues. Several studies have found that the permittivity of cancerous breast tissue is higher than normal breast tissue and also higher than non-malignant tumours [3, 4]. Disease and injuries might lead to changes in dielectric properties. A possible example is the coagulation of blood while bleeding [2]. Another example is the case during an ischemic stroke where the dielectric properties will change due to the loss of circulation [5]. With the proper choice of the frequency, microwave signals can penetrate deeply into the body, and sense the change of dielectric properties due to disease or tissue abnormalities.

Although highly promising, most of the relevant research are so far proof of concept using costly and bulky lab instrument, e.g. vector network analysers (VNAs) or oscilloscopes. In order to enable clinical adaptation, compact and low-cost measurement systems are required. In the last few years, several research groups have started working on the minimisation of systems either with custom design or using compact commercial instrument. A compact VNA with largely reduced size was employed in work [6–9] to facilitate the clinical trials. Paper [10] presented a custom designed ultra-wideband (UWB) radar transceiver dedicated for breast imaging based on CMOS technology. Popovic et al. reported their work on the minimisation of a time domain breast imaging system through the integration of the switching matrix with the antenna array [11]. They recently published their work on introducing an integrated circuit (IC) pulse radio as a replacement for the bulky and expensive pulse generator [12]. We, as one of the leading research groups working on microwave-based medical diagnostics, have also made much effort on the development of miniaturised systems with the long-term goal of having a system-on-chip [13, 14].

Most recently, a new type of system that has been commonly employed in radio communications, e.g. multiple input and

multiple output (MIMO) wireless systems [15], has attracted interest of our researchers in this community. This system is based on software defined radio technology (SDR) and the whole system is built on a single circuit board which consists of a radio frequency integrated circuit (RFIC) transceiver and a digital signal processing (DSP) unit. The system is compact, cheap, and portable. Moreover, the system is a highly flexible and generic measurement platform for many different medical applications as it allows the adjustment of various system parameters, such as the output power, working frequency, receiver gain, sampling rate etc.

Marimuthu et al. proposed a SDR based ultra wideband medical imaging system working in monostatic mode and reported successful imaging results of simple objects [16]. The same research group has also developed a multistatic imaging system composed of the SDR board and a switching matrix [17]. A sixteen channel tomographic system that is composed of nine SDR boards was recently reported by Meaney et al. This multiple board system was dedicated for breast imaging, and it was claimed that the system is able to measure a signal as low as −140 dBm [18]. However, most of the relevant work reported so far were mainly focused on system development with little investigation on the measurement quality.

Measurement quality is a big concern for medical diagnostics. Due to the high-lossy characteristics of biological tissues, the received signal are usually very weak, and the reliable detection of tissue abnormalities and diseases relies largely on the high quality measurement. We have previously demonstrated that when the measurement error of a medical imaging system exceeds a certain level, the reconstructed image became distorted [19]. It is therefore very important to have a good knowledge of the system and have a clear picture on the achievable measurement accuracy in order to develop a successful medical diagnostic system for specific applications. In ref. [20] Meaney et al. has discussed a few aspects related to the measurement quality but the discussion was based on a multi-board SDR system, which is complicated and not applicable for prehospital medical diagnostics due to the big size.

In this work, we will perform an extensive investigation on the measurement quality of a single SDR board based system, mainly dedicated to prehospital medical diagnostics applications where the system size, cost, and measurement speed are of vital importance. We will focus on statistical measure of the measurement quality in both amplitude and phase over a frequency band 500 MHz–2 GHz and benchmark the system against a high performance VNA. We will evaluate the effectiveness of a proposed calibration approach and discuss different factors/parameters that affect the measurement quality.

The rest of the paper is organised as follows. In Section 2, the system architecture, working principle and the proposed measurement scheme of a SDR system were presented. In addition, the accuracy related issues were analysed and the performance of metrics were introduced. The fundamental performance of a SDR board was investigated and presented in Section 3. In order to deal with the phase randomness problem, a calibration strategy was proposed in Section 4 and the effectiveness was demonstrated. The obtained performance was further verified by the measurement of an antenna system for medical diagnostics in Section 5. Section 6 discusses the factors/parameters that affect the measurement quality of the SDR board and a conclusion was drawn in the last section.

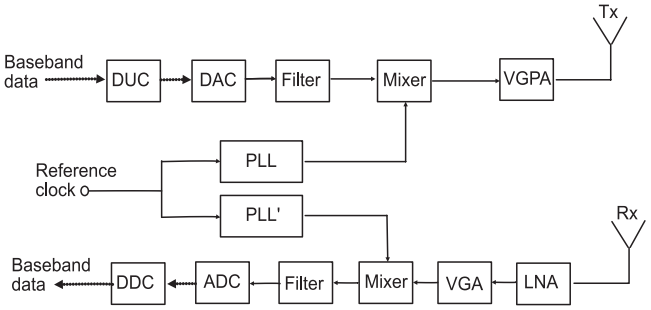

FIGURE 1 The principal block diagram of a typical SDR system

2 | SOFTWARE DEFINED RADIO SYSTEM: PRINCIPLE AND ACCURACY CONCERN

The traditional microwave hardware based devices have the problem that they can only be modified through physical intervention. This can result in an increased production cost and reduced flexibility in support of new standards. The advantage of using SDR is that it presents an efficient and inexpensive solution to all the problems of the traditional hardware based devices. In the SDR the physical layer processing is carried out through adaptable software operating on programmable processing technologies, this includes the field programmable gate arrays (FPGA), digital signal processor (DSP), general purpose processors (GPP) and programmable system in chip (SoC). This allows new features to be added to existing systems without requiring adding new hardware. This type of system provides a broad range of system gain variation, and it allows the adjustment of different parameters for achieving a good trade-off between measurement quality and measurement speed. All these features are favourable for medical diagnostics.

2.1 | System architecture and principle

Figure 1 presents the principal block diagram of a typical one channel software-defined radio system for medical applications. The transmitter consists of a digital up converter (DUC), a digital to analogue converter (DAC), a filter, a mixer and a variable gain power amplifier (VGPA). The components in the receiver are similar to those in the transmitting channel, including a low noise amplifier (LNA), a variable gain amplifier (VGA), a mixer, a filter, an analogue to digital converter (ADC) and a digital down converter (DDC). Two different phase locked loop (PLL) synthesisers work as local oscillators to the mixers in the transmitter and receiver respectively.

With this system, a baseband signal, which is usually a single tone, is created in digital domain. This digital signal will firstly

be interpolated through the DUC and then be converted to analogue signal by the DAC. The analogue signal will then be further filtered, modulated to a higher frequency, and amplified before being transmitted out by an antenna. The received signal will go through a similar process but in a reversed order. It will firstly be amplified with a certain gain depending on its strength and then be down converted to an intermediate frequency in order to facilitate the analogue to digital conversion. The obtained digital data will be further downsampled by the DDC before being transferred to a PC for processing.

With a stepped frequency approach, wide band measurements can be performed. As there are variable gain amplifiers in both the transmitter and the receiver, the system can potentially give a very high dynamic range. This makes it very suitable for medical diagnostics, where the received signals may vary a lot in terms of signal strength.

2.2 | Measurement scheme

Unlike the previous work [16, 20], where the baseband signal is a single tone having a frequency value of a few kHz, we used direct current (DC) data instead in order to imitate the operation of a typical vector network analyser.

This DC signal is modulated with a carrier frequency and amplified before being transmitted out. The transmitted signal can be expressed as the following:

$$\begin{aligned} T_x(t) &= [A_{\mathrm{I}} \cdot \cos(2\pi f_c t + \phi_{tx}) + A_{\mathrm{Q}} \cdot \sin(2\pi f_c t + \phi_{tx})] \cdot G_t \\ &= G_t \cdot A \cdot \cos(2\pi f_c t + \theta + \phi_{tx}) \end{aligned} \tag{1}$$

Where A_{I} and A_{Q} are the magnitudes of the DC baseband data in I channel and Q channel respectively, f_c is the transmitted frequency, ϕ_{tx} is the added phase from the transmitter and G_t is the transmitter gain. The amplitude $A = \sqrt{A_{\mathrm{I}}^2 + A_{\mathrm{Q}}^2}$ and the angle $\theta = \arctan(A_{\mathrm{Q}}/A_{\mathrm{I}})$. The signal is transmitted by an antenna into an object under test (OUT), and the reflected or transmitted signal acquired by the receiving antenna can then be expressed as:

$$R_x(t) = G_t \cdot A \cdot e_p \cdot \cos(2\pi f_c t + \theta + \phi_{tx} + \phi_p) \tag{2}$$

Where the parameter e_p and ϕ_p are used to characterise the amplitude and phase change of the signal due to antenna and propagation effect. This acquired signal will be amplified, mixed down and filtered to result in an intermediate frequency component according to the following:

$$\begin{aligned} R_{\mathrm{I}} &= R_x(t) \cdot G_r \cdot \cos(2\pi f_0 t + \phi_{rx}), \\ R_{\mathrm{Q}} &= R_x(t) \cdot G_r \cdot \sin(2\pi f_0 t + \phi_{rx}) \end{aligned} \tag{3}$$

Here R_{I} and R_{Q} represent for the intermediate frequency signal in I channel and Q channel respectively. f_0 is the frequency generated by the local oscillator of the receiver, G_r is the receiver gain and ϕ_{rx} is the added phase from the receiver. We assume an ideal IQ balance, i.e. the gain and phase are the same in both channels. The board has an analogue filter for eliminating DC components and in order to acquire a DC signal, the LO frequency needs to be configured different from the carrier frequency. The frequency f_0 was a few MHz offset to the transmitting frequency f_c so that the intermediate frequency signal is in the passband of the filter. The filtered signal will then be converted to digital signal, which is further down converted to DC component in digital domain with the DDC. Combing Equations (2) and (3) and taking into account measurement noise, the received data can be expressed as:

$$\begin{aligned} I_{\mathrm{DC}}(n) &= G_t \cdot G_r \cdot e_p \cdot A \cdot \cos(\theta + \phi_p + \phi_{tx} - \phi_{rx}) + n_{\mathrm{I}}(n), \\ Q_{\mathrm{DC}}(n) &= G_t \cdot G_r \cdot e_p \cdot A \cdot \sin(\theta + \phi_p + \phi_{tx} - \phi_{rx}) + n_{\mathrm{Q}}(n), \end{aligned} \tag{4}$$

Here I_{DC} and Q_{DC} are the DC data acquired from I channel and Q channel respectively. n_{I} and n_{Q} represent the overall measurement noise, which includes the effect of nonlinearity, thermal noise from the hardware, jitter resulted noise etc.

2.3 | Accuracy concern

The software defined ratio system is frequency domain based. Although it is flexible and powerful, we foresee several issues that limit the measurement quality.

The first is the signal leakage from the transmitter to the receiver. Transmitter leakage may be coupled from one conducting path to another or may result from crosstalk leaking through integrated circuits substrates, device packages or printed circuit boards. The leakage signal from the transmitter will add up to the received signal of interest, leading to degraded signal to noise ratio.

The second is the measurement stability. Stable measurement over a time period is of vital importance for medical diagnostics, especially for monitoring purposes. A software-defined radio system is a combined system design consisting of both analogue and digital circuits, and the measurement stability is not only affected by the thermal noise from analogue components but also the stability of digital circuits, such as timing sources.

The third is the phase incoherence. In some diagnostic applications, especially those where an imaging result is preferred, accurate measurement of both amplitude and phase are desired. In the SDR system, the carrier frequencies of the transmitter and receiver are generated by two different PLLs. Although they have the same reference input clock, the output clock signals are not synchronised, and the phases of the generated clocks are random and vary from run to run. This not only results in frequency offset error but also a random phase offset between the transmitter and receiver. As a consequence, the measured phase will also be random and cannot be correlated to the object response.

2.4 | Measurement repeatability and accuracy

Measurement repeatability and measurement accuracy are the two performance of metrics that will be used to evaluate the measurement quality of a SDR system. Measurement repeatability, also named as signal to noise ratio (SNR), is used to characterise the measurement stability of the system, and it indicates the consistence of the measurement over a period of time. It is the most relevant performance of metric for our approach [6] as the clinical decision usually relies on the change of measurement data over a period or comparison among a large data set. A system with poor measurement repeatability cannot reliably present the small difference in the measurement data due to pathological change.

According to the model described in Section 2.2, the magnitude of the received signal can be written as:

$$R_{\mathrm{DC}}(n) = \sqrt{I_{\mathrm{DC}}^2(n) + Q_{\mathrm{DC}}^2(n)} \tag{5}$$

The measurement repeatability at each frequency is then calculated from a number of repetitive measurements according to the following:

$$\mathrm{MR} = \frac{\overline{R}}{\sqrt{\frac{1}{N}\sum_{k=1}^{N}[R_k - \overline{R}]^2}} \tag{6}$$

where N is the number of repetitive measurements, R_k is the obtained magnitude (one sample or the average of a number of samples of R_{DC}) or phase from the kth measurement, and $\overline{R}$ is the mean of the amplitudes or phases from N repetitive measurements.

Measurement accuracy indicates how close the measurement data is to the actual value, and it reflects the measurement quality of an absolute measurement. Since the actual value are usually unknown, a high performance VNA is commonly used to provide a ground truth.

In the following sections, the measurement quality of a specific SDR system will be investigated over the most interested frequency range for medical diagnostics: 500 MHz–2 GHz.

3 | PERFORMANCE OF A SOFTWARE DEFINED RADIO SYSTEM

The investigated system is a two-channel SDR board USRP2901 from National Instruments [21] and this board is equivalent to Ettus Research USRP B210. The system operates from 70 MHz to 6 GHz and has a maximum instantaneous bandwidth of 56 MHz. The transmitter gain range and receiver gain range of the SDR board are 89.75 dB (−40 to 49.75 dB) and 76 dB (−15–61 dB) respectively. In each channel, there are two RF ports. One port can be configured as either transmitting or receiving port and the other port is receiving only. The transmitters of the two channels share one local oscillator (LO) and the receivers from both channels share another LO. In order to minimise the signal leakage, we configured the transmitting port of one channel (channel 1) as transmitter and the receiving port of the other channel (channel 2) as receiver, as shown in Figure 2(a). Labview was used as the development platform for all the test and measurement.

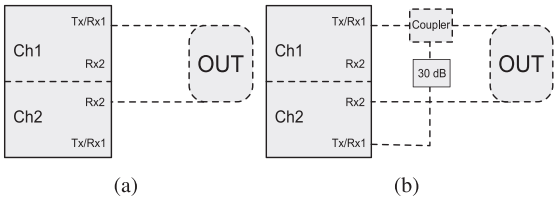

FIGURE 2 The measurement setup for (a) uncalibrated measurement and (b) calibrated measurement

TABLE 1 System parameters used in measurements unless otherwise stated

Parameters	Value
IQ rate	100 kS/s
Tx gain (G_t)	15 dB
Rx gain (G_x)	−15 dB
Carrier frequency (f_c)*	500 MHz–2 GHz
LO frequency (f_0)	f_c-5 MHz
DAC sampling rate	61.44 MS/s
ADC sampling rate	61.44 MS/s
Transmitted amplitude	1 V
Number of samples	16,384

*Carrier frequency f_c sweeps from 500 MHz to 2 GHz with a step size of 100 MHz.

The parameters used in the following work were given in Table 1 unless otherwise stated. The IQ rate was set to 100 kS/s in order to obtain a low Nyquist noise level and the sampling rate for both the DAC and ADC is 61.44 MS/s. The interpolation and decimation factors were automatically set by the SDR software based on the user specified IQ rate. The receiver is set to −15 dB in order to keep the receiver noise minimum. The transmitter gain is 15 dB to make the receiver work in a linear mode over the frequency range of interest. The LO frequency is 5 MHz offset from the carrier frequency, and this value is high enough so that the aforementioned filter will not filter the mixer output out, but still close enough that the bandwidth of the digital signal processor will be able to process the remaining signal.

3.1 | Linear operation region

In order to get a picture of linear operation region for both the transmitter and the receiver, two different measurements were performed. In the first measurement we connected a 30 dB attenuator between the transmitter and receiver with a cable, set the receiver gain $G_r = -15$ dB and adjusted the transmitter gain. This measurement was done to estimate the maximum

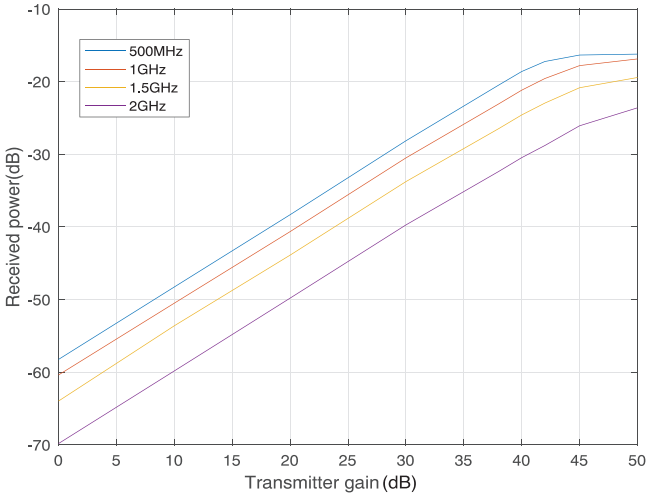

(a)

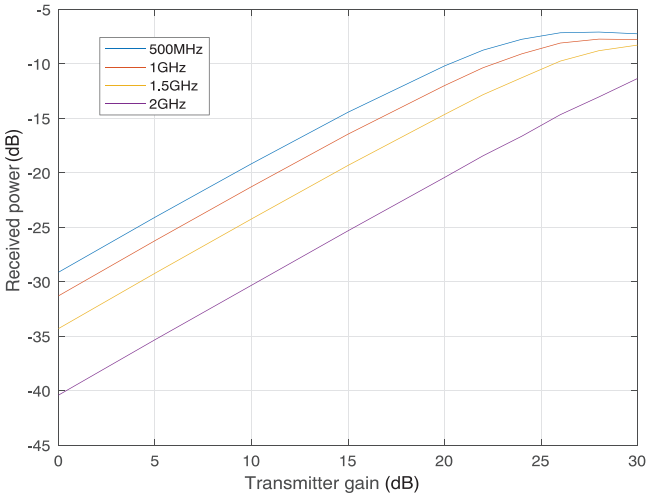

(b)

FIGURE 3 The measured power when (a) a 30 dB attenuator was connected between the transmitter and receiver and (b) when the transmitter and receiver were connected with a short cable

transmitted power. We keep the receiver gain minimum in order to minimise the receiver noise level. The 30 dB attenuator was used in order to make sure that the received power would not reach the saturation region of the receiver. Figure 3(a) shows the measured power at a few discrete frequencies versus transmitter gain. It can be seen that the saturated power levels differ for different frequencies, and the frequency 500 MHz becomes clearly saturated when the transmitter gain is larger than 40 dB. When the transmitter gain is less than 40 dB, the transmitter presents a good linearity within the interested frequency range. It should be noted that the power was calculated as the square of the received DC magnitude, as expressed in Equation (5), without taking into account a 50 ohm load, and this calculation applies to the rest of this paper.

The linear operation region of the system is not only affected by the linearity of the transmitter but also the receiver. In order to estimate the linear region of the receiver, we took away the 30 dB attenuator and performed a similar measurement as

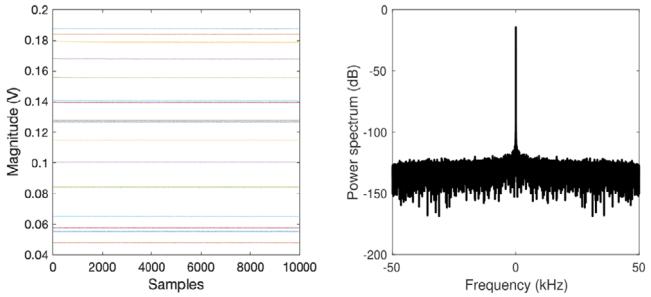

(a) (b)

FIGURE 4 The obtained baseband data when the transmitted frequency is 500 MHz: (a) baseband samples (b) power spectrum

earlier. Figure 3(b) shows the received power versus transmitter gain, which indicates that the receiver starts saturating when the transmitter gain is over 15 dB.

3.2 | Maximum received power and signal leakage

We set the transmitter gain $G_t = 15$ dB and measured the received power at frequencies from 500 MHz to 2 GHz with a frequency step 100 MHz. Figure 4(a) shows the recorded DC samples for all the frequencies and Figure 4(b) is the obtained power spectrum when the transmitted signal is 500 MHz. It can be seen that the received power at 500 MHz is about -15 dB and the noise floor is about -120 dB/Hz. This gives a good estimate of the strongest signal that the receiver can handle with good linearity.

In order to estimate the signal leakage from the transmitter to the receiver, a similar measurement was performed when the transmitter and receiver were disconnected, and all the ports are terminated with a 50 ohms load. The receiver in the same channel as the transmitter was also considered in this measurement. The leakage power is plotted in Figure 5 in comparison with the maximum received power obtained from the previous measurement. We can clearly see that the signal leakage from the transmitter to the receiver that is in a different channel is much lower, especially within the frequency range 1–1.7 GHz. A dynamic range of about 75–85 dB can be achieved within the interested frequency range when the transmitter and receiver are configured in different channels if only considering the signal leakage.

3.3 | Measurement repeatability

In a microwave based medical diagnostic system, the signals acquired by different antennas can vary a lot in strength and therefore have different measurement quality. In order to imitate a typical medical diagnostic measurement scenario, we connected a variable attenuator with adjustable range of 70 dB between the transmitter and receiver, and investigated

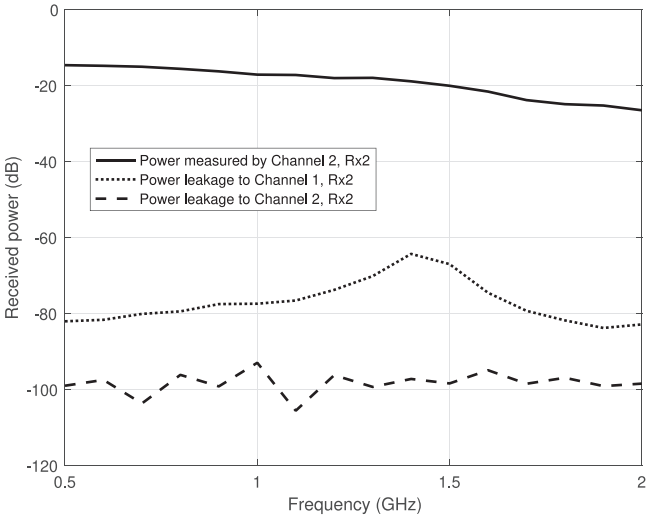

FIGURE 5 The maximum received power when the system operates in the linear region and the power leakage from the transmitter to the receiver

the measurement repeatability when the attenuation are at different levels.

Thirty repetitive measurements were performed when the attenuator was set as 0, 30, 50, and 70 dB respectively. Figure 6(a) shows the measured power from the thirty repetitive measurement for different attenuation levels. It can be clearly seen that the variation of measured power from repetitive runs increases with the attenuation level. The corresponding measurement repeatability calculated according to Equation (6) were shown in Figure 6(b) when one sample and the average of one thousand samples were used to represent the received magnitude. The results show that when 1000 samples were used instead of one sample, the measurement repeatability is better for attenuation levels 30, 50, 70 dB, but not 0 dB. This indicates that when the received signal is very strong (e.g. when the attenuation is 0 dB), the error sources that limit the measurement quality is not the additive thermal noise, but something else, e.g. the linearity. That's why the measurement repeatability cannot be further improved by means of sample averaging. Nevertheless, the mean of 1000 samples will be used in the following work.

The results also show that there is a much smaller increase of the measurement repeatability for frequencies around 700 MHz when more samples are used. A possible explanation is that although the averaging of more samples results in a decreased additive noise, but other errors become more significant as more samples were taken into account for some discrete frequencies. It can also been seen that averaging does not contribute to a higher measurement repeatability at the higher frequencies when the attenuation is 70 dB. This is because the signal became too small and was immersed in the noise, which results in almost the same SNRs due to the numerical error.

As aforementioned, the measured phase exhibits a random manner, which is clearly illustrated in Figure 7 where the measured phase from five repetitive measurements were plotted together. This can be well understood and expected according

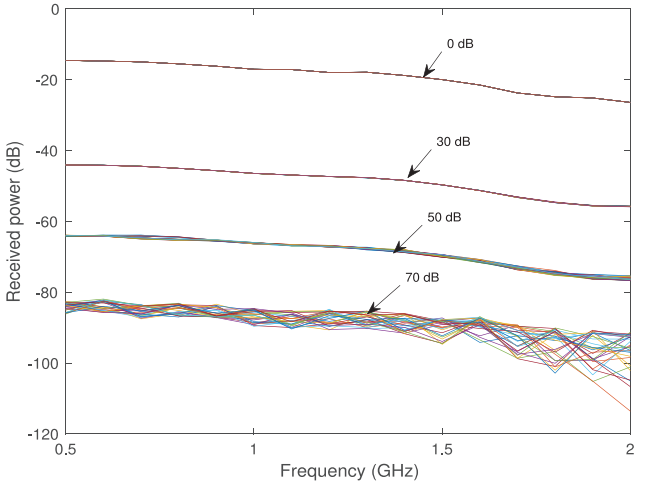

(a)

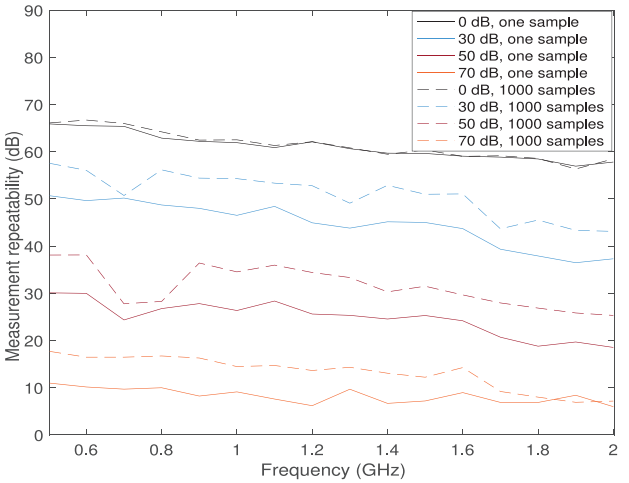

(b)

FIGURE 6 Uncalibrated measurement of a variable attenuator: (a) measured power and (b) measurement repeatability for different attenuation levels

to Equation (4) since both the transmitter phase and receiver phase components are random from run to run and cannot be correlated to the object response in a determined way.

4 | CALIBRATION FOR PHASE COMPENSATION

In order to obtain a stable phase measurement, the random phase generated by the PLLs under each measurement needs to be determined and compensated. The conventional calibration approach for a VNA, where the calibration measurement is done in a different run from the real measurement of interest, is not applicable here since the generated phases vary from run to run. The key is to perform the calibration measurement and object measurement under the same run so that the random phase can be obtained and be compensated for.

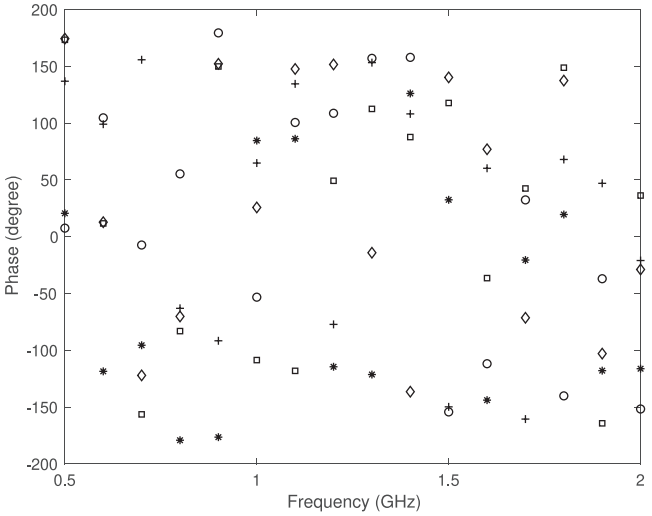

FIGURE 7 The measured phase at different frequencies under five repetitive measurements. The obtained phase from each measurement are represented by a different marker

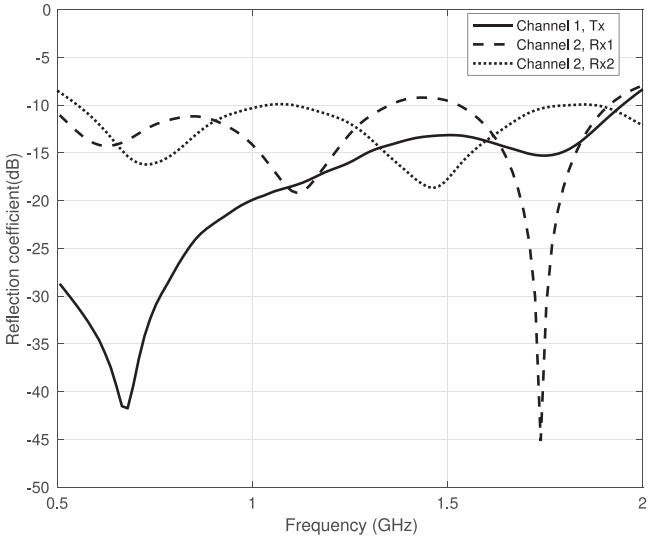

FIGURE 8 The reflection coefficients of the transmitting port and the receiving ports

The simplest solution is creating a reference channel and an object channel using the two receivers since they are sharing the same PLL and the generated clock phase are the same for both receivers. However, the efficacy of this solution relies on the performance of both receivers and is largely affected by the high signal leakage from the transmitter to the receiver in the same channel according to Figure 5.

The fact that the receiver of this SDR board can be connected to two different receiving ports with an internal switch facilitates a better solution by using the same receiver for both reference and object measurement, as shown in Figure 2(b). In order to ensure a good outcome of this solution, the key is to minimise the interference between the reference channel and the object channel.

Figure 8 shows the reflection coefficient of the transmitting port and the two receiving ports when they were configured in active mode. Although the reflection coefficient of all the ports are below −10 dB at most of the frequencies, the signal reflection at the receiving ports is relatively high in comparison with a well matched load. This will result in a multiple reflection scenario and makes it challenging to achieve a good isolation between the reference channel and object channel. We therefore used a directional coupler with directivity about 30 dB to separate the reference channel and object channel. A 30 dB attenuator was added in the reference channel in order to further reduce the reflected signal leakage from the reference channel to the object channel. We used 30 dB because it is close to the lowest signal attenuation level in a typical medical diagnostic scenario, and a too high attenuation will result in a poor SNR, affecting the calibration accuracy negatively.

The same variable attenuator was measured and Figure 9 shows the recorded DC samples from the reference channel and object channel when the attenuator was set at 30 dB. An abrupt change in the signal magnitude appears some time after the recording starts in Figure 9(b) and this indicates a delay

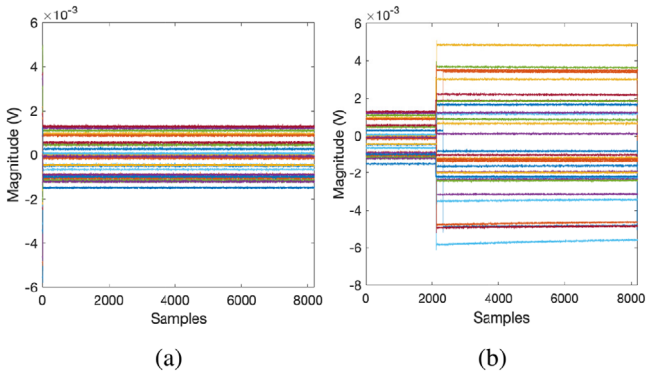

FIGURE 9 The obtained DC samples from (a) the reference channel and (b) the object channel

(about 0.02 s) between the switch command and action. The signal level from the reference channel is lower than that from the object channel as the attenuation in the reference channel is about 40 dB (a 30 dB attenuator plus 10 dB coupling) in total.

Repetitive measurements were carried out for different attenuation levels, and Figure 10(a) shows the received power in the object channel from thirty repetitive measurements. The results are very similar to those shown in Figure 6(a), which indicates little interference from the reference channel to the object channel. The ground truths, which were obtained from VNA measurement, were also plotted in this figure to demonstrate the measurement accuracy of the SDR measurement. The results show a very good agreement between the SDR measurement and the ground truth when the attenuation level are 30 and 50 dB. As the attenuation increases further to 70 dB, the measured signals vary much from run to run but are still well bounded to the ground truth for frequencies below 1.5 GHz. Over 1.5 GHz, the signal variation increases significantly, resulting in a poor measurement accuracy.

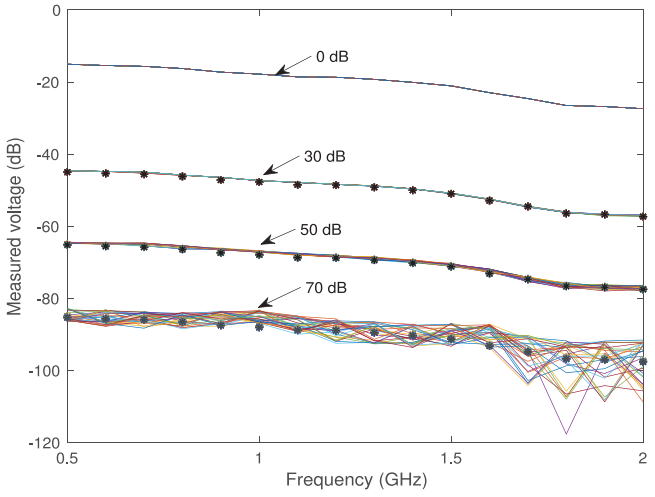

(a)

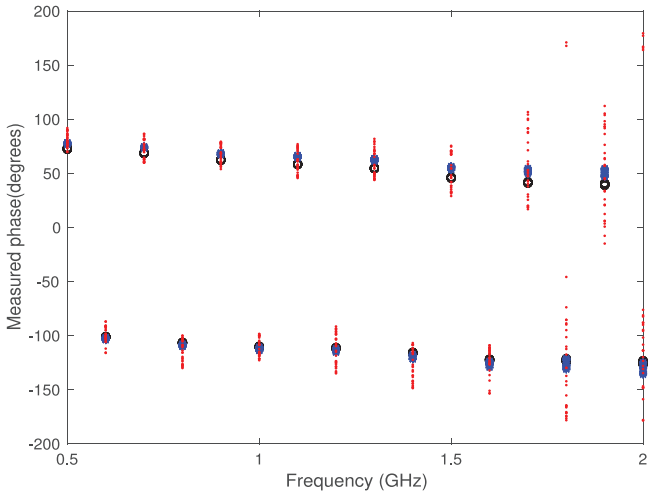

(b)

FIGURE 10 Calibrated measurement of a variable attenuator: (a) measurement quality of amplitudes and (b) obtained phases from 30 repetitive measurements. The black stars represent the ground truth obtained from VNA measurements. The black circles, blue stars and red dots are the measured phases when the attenuation level was 30, 50, and 70 dB respectively

We took the difference of the measured phase from the object channel and the reference channel, and the obtained results were shown Figure 10(b) for the thirty repetitive measurements when the attenuation level are 30, 50, and 70 dB respectively. In comparison with Figure 7, we can see that a relative consistent phase was obtained from run to run and the consistency is better when the attenuation level is lower. This is in a good agreement with the amplitude measurement results.

5 | ANTENNA SYSTEM MEASUREMENT

An antenna system was measured in order to further verify the measurement accuracy. The antenna system is a circular array composed of 16 monopole antennas and placed in an imaging tank. In order to eliminate the interference due to multiple scattering effect, the antennas were immersed in a lossy media. Two different antenna pairs were measured with the SDR system and a Rohde & Schwarz VNA respectively. In order to calculate the transmission coefficient from the SDR measurement data, a reference measurement was done by connecting the transmitting and receiving ports with a short cable.

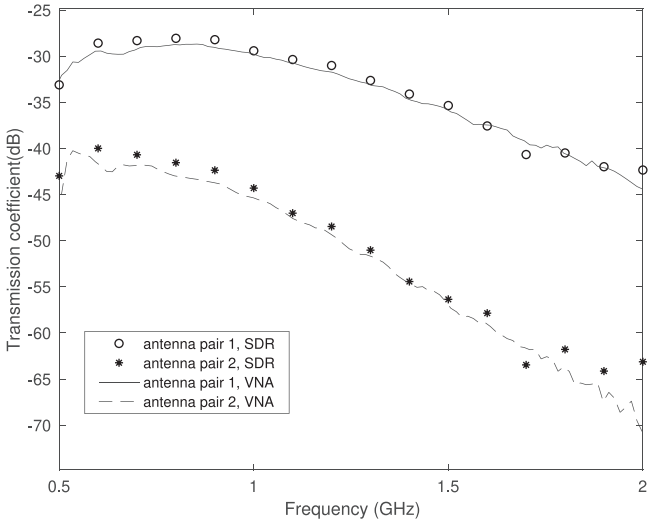

FIGURE 11 Comparison of the transmission coefficients of two antenna pairs measured with the SDR system and the VNA respectively. The solid line and the dashed line represent the transmission coefficient measured with the VNA. The star and the circle are the transmission coefficient obtained from the SDR measurement

The obtained transmission coefficient, which is the ratio of the received power from antenna measurement to that from reference measurement, were plotted in Figure 11 in comparison with VNA data. The solid line and the dashed line represent the transmission coefficient measured with the VNA. The star and the circle are the SDR measurement data. It can be seen that the transmission coefficient measured by the SDR starts to deviate from the VNA data when the transmission level approaches 70 dB, indicating decreased measurement accuracy. This is in good agreement with the results shown in Figure 10(a).

6 | DISCUSSION

It is worth noting that the results presented in this work were obtained under specific settings. The measurement quality of the SDR system is dependent on many parameters.

One of them is the IQ rate. A lower IQ rate entails a narrower decimation filter. This will result in a lower noise power due to the reduced Nyquist noise bandwidth [22] but on the other hand increases the measurement time. The IQ rate used in this work is 100 K samples/s, which is almost the least allowable IQ rate of the SDR system.

The number of samples can also affect the measurement quality in a way that averaging the samples can improve the signal to noise radio (SNR) due to additive thermal noise, which was shown in Figure 6(b). However, the results also suggested

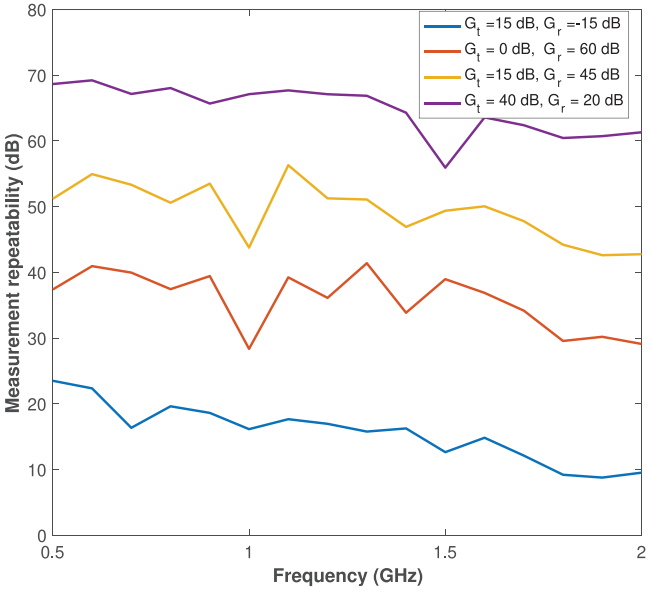

FIGURE 12 Measurement repeatability of a 60 dB attenuator obtained with the SDR board when different gain settings were used. No averaging of samples was applied for this measurement

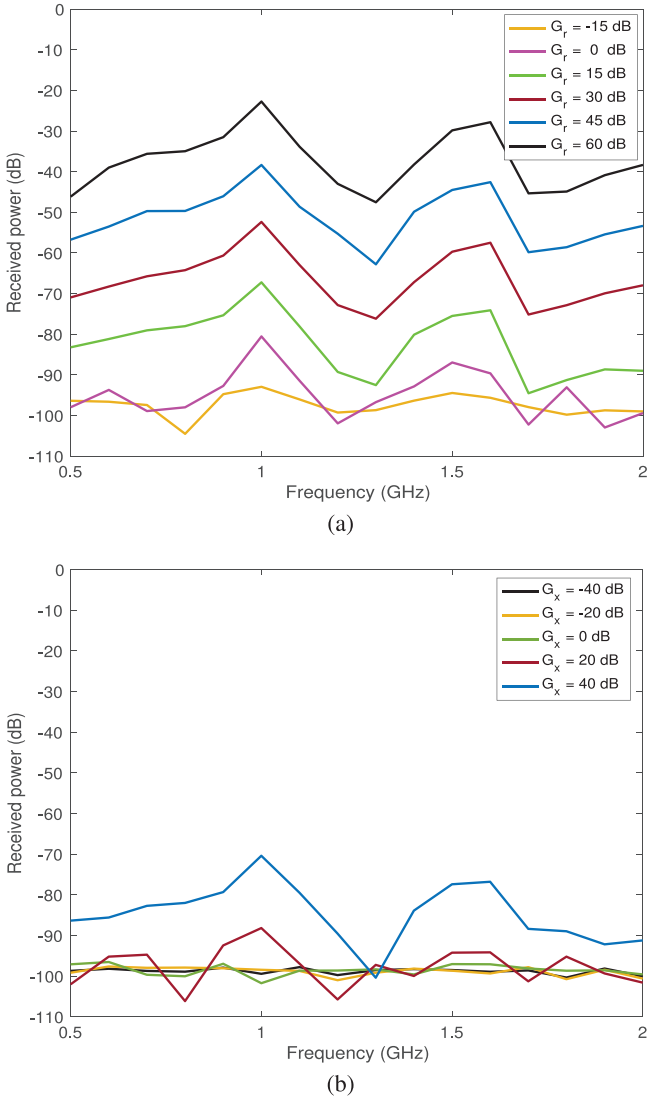

FIGURE 13 Power leakage from the transmitter to the receiver as (a) the receiver gain increases and the transmitter gain $G_t = 15$ dB, (b) the transmitter gain increases and the receiver gain $G_r = -15$ dB

that the averaging of samples may not be effective for all the frequencies due to other accumulated errors, e.g. nonlinearity.

Other important parameters that affect the measurement quality are the transmitter gain and the receiver gain as both can promote the strength of the received signal, which may result in a better signal to noise ratio. In this work, it was assumed that no priori information of the measured objects were known and the gain values were determined to ensure a linear operation mode with the highest possible receiving power and lowest receiver noise over frequency range 500 MHz–2GHz. With a good knowledge of the measured object, e.g. the transmission loss level, a dedicated transmitter gain or receiver gain can be used to strengthen the received signal, resulting in a higher SNR. One measurement example was demonstrated in Figure 12. The figure shows the measurement repeatability of a 60 dB attenuator when different gain settings were applied. The blue line represents the obtained measurement repeatability when the same gain settings as in Figure 6 were used. In order to compensate for the 60 dB transmission loss, an extra 60 dB gain was added to the original gain settings and three different gain settings: ($G_t = 15$ dB and $G_r = 45$ dB), ($G_t = 0$ dB and $G_r = 60$ dB), ($G_t = 40$ dB and $G_r = 20$ dB) were considered. It can be seen that the measurement repeatability becomes much better as the gain increases. The results also suggest that the improvement on the measurement repeatability is more significant by increasing the transmitter gain instead of the receiver gain. This is because increasing the receiver gain will also lead to an increased receiver noise. When the $G_t = 40$ dB and $G_r = 20$ dB, the SNR can reach up to 70 dB at the low frequency region and this performance is similar to that reported in ref. [20], which claimed a SNR about 75 dB at the frequency 1300 MHz for a 50 dB attenuation level.

Although the measurement repeatability of a highly lossy object can be improved by using higher gain settings, it needs to be noted that this measure will also result in worse power leakage, as shown in Figure 13. This figure presents the level of the leaked power from the transmitter to the receiver as the transmitter gain or receiver gain increases. Figure 13(a) shows the leakage power when increasing the receiver gain while keeping the transmitter gain $G_t = 15$ dB. Figure 13(b) presents the change of the leaked power level as the transmitter gain increases and the receiver gain $G_r = -15$ dB was kept unchanged. The maximum considered transmitter gain was 40 dB as beyond this value the SDR board will work in a nonlinear mode, as demonstrated in Section 3.1. The results show that the power leakage increases nearly linear with the receiver gain when the gain changes from 0 to 60 dB while there is little difference in the leakage power when the transmitter gain increases from −40 to 0 dB. This indicates that it is beneficial to use a higher transmitter gain even from the perspective of power leakage. The maximum output power level of the SDR board is

about 8 dBm [23], which is much lower than the radiated power level of a cell phone and is thus considered be safe for human.

The investigated frequency range 500 MHz–2 GHz is optimal for stroke and brain trauma diagnostics [6] in consideration of the significantly reduced penetration depth at higher frequencies. For other medical applications, such as breast imaging, the preferred frequencies were under 3 GHz in tomographic methods while much higher frequencies (e.g. 2–16 GHz) were used in radar-based methods in order to obtain a sufficient bandwidth [24]. It is then important to be noted that the transmitted power of the SDR board decreases dramatically versus frequency over the entire operation band (70 MHz–6 GHz), which makes it challenging to obtain good accuracy at higher frequencies. A possible solution is to adapt the gain to each frequency, but this will largely increase the measurement complexity in terms of operation and calibration.

The focus of this work is to give a picture of the measurement quality of a low cost and compact SDR board. In order to make the investigation relevant to medical diagnostics, a measurement was performed on a variable attenuator with 70 dB adjustable attenuation range with the purpose of imitating a typical measurement scenario in medical diagnostics. In addition, an antenna system dedicated for breast imaging was also investigated. It is not a trivial task to answer if the achieved measurement quality is good enough for different medical applications as the required measurement accuracy for a specific application depends on the performance of algorithm, the dielectric contrast of the object etc. Our previous work showed that a SNR over 15 dB is sufficient for the reconstruction of a specific breast model by using a time domain tomography approach [19]. This level of accuracy can be achieved with the investigated SDR board. More extensive investigation on the sensitivity of different medical applications to the measurement error is beyond the scope of this work.

The measurement repeatability shown in Figure 6(b) is comparable to that of the custom-developed time domain system presented in ref. [14] but with a much lower transmitted power. This performance is superior to a pulsed time domain system which usually has a maximum SNR about 40 dB in the investigated frequency range [13]. In the future, it is interesting to look into the calibration approach in order to further improve the performance. The effectiveness of the calibration is mainly affected by the isolation between the reference channel and object channel. Although good performance was demonstrated with the proposed solution, further effort on minimising the isolation can lead to better measurement accuracy. Other interesting future work includes using two SDR boards to eliminate the power leakage problem and comparing the performance that can be obtained with different SDR platforms.

7 | CONCLUSION

Good measurement repeatability and measurement accuracy of the investigated SDR board were demonstrated by benchmarking against a high performance VNA for a transmission loss up to 70 dB, which is sufficient for most of the diagnostic applications. With the priori information of the transmission loss level in a specific diagnostic scenario, good accuracy can be achieved for even higher transmission loss by adapting the system gain. To achieve the best measurement quality, it is beneficial to use a high transmitter gain instead of the receiver gain and the highest achievable measurement accuracy is mainly limited by the power leakage from the transmitter to the receiver.

AUTHOR CONTRIBUTIONS

Xuezhi Zeng: Conceptualization, data curation, formal analysis, investigation, methodology, resources, supervision, validation, visualization, writing - original draft, writing - review and editing. Laura Orozco: Data curation, investigation, software.

ACKNOWLEDGMENT

This work was supported by the Swedish Agency for Innovation Systems within the Chalmers Antenna Systems VINN Excellence Centre (Chaseon).

CONFLICT OF INTEREST

The authors declare no conflict of interest.

DATA AVAILABILITY STATEMENT

Data available on request from the authors

ORCID

Xuezhi Zeng https://orcid.org/0000-0002-6606-0386

REFERENCES

1. Rosen, A., Stuchly, M.A., Vorst, A.V.: Applications of RF/microwaves in medicine. IEEE Trans. Microwave Theory Tech. 50(3), 963–974 (2002)
2. Fhager, A., Candefjord, S., Elam, M., Persson, M.: Microwave diagnostics ahead: saving time and the lives of trauma and stroke patients. IEEE Microwave Mag. 19(3), 78–90 (2018)
3. England, T.S.: Dielectric properties of the human body for wave-lengths in the 1–10 cm range. Nature 166, 480–481 (1950)
4. Surowiec, A.J., Stuchly, S.S., Barr, J.R., Swarup, A.: Dielectric properties of breast carcinoma and the surrounding tissues. IEEE Trans. Biomed. Eng. 35(4), 257–263 (1988)
5. Semenov, S., Huynh, T., Williams, T., Nicholson, B., Vasilenko, A.: Dielectric properties of brain tissue at 1 GHz in acute ischemic stroke: experimental study on swine. Bioelectromagnetics 38(2), 158–163 (2016)
6. Persson, M., Fhager, A., Trefna, H.D., et al.: Microwave-based stroke diagnosis making global prehospital thrombolytic treatment possible. IEEE Trans. Biomed. Eng. 61(11), 2806–2817 (2014)
7. Mobashsher, A.T., Abbosh, A.M., Wang, Y.: Microwave system to detect traumatic brain injuries using compact unidirectional antenna and wideband transceiver with verification on realistic head phantom. IEEE Trans. Microwave Theory Tech. 62(9), 1826–1836 (2014)
8. Candefjord, S., Winges, J., Malik, A.A., et al.: Microwave technol-ogy for detecting traumatic intracranial bleedings: tests on phantom of subdural hematoma and numerical simulations. Med. Biol. Eng. Comput. 55, 1177–1188 (2016)
9. Ljungqvist, J., Candefjord, S., Persson, M., et al.: Clinical evaluation of a microwave-based device for detection of traumatic intracranial hemorrhage. J. Neurotrauma 34, 2176–2182 (2017)
10. Bassi, M., Caruso, M., Khan, M.S., Bevilacqua, A., Capobiano, A.-D., Neviani, A.: An integrated microwave imaging radar with planar antennas for breast cancer detection. IEEE Trans. Microwave Theory Tech. 61(5), 2108–2118 (2013)

11. Santorelli, A., Porter, E., Kang, E., Piske, T., Popovic, M., Schwartz, J.D.: A time domain microwave system for breast cancer detection using a flexible circuit board. IEEE Trans. Instrum. Meas. 64(11), 2986–2994 (2015)
12. Kranold, L., Taherzadeh, M., Nabki, F., Coates, M., Popović, M.: Microwave breast screening prototype: system miniaturization with IC pulse radio. IEEE J. Electromagn. RF Microwave Med. Biol. 5(2), 168–178 (2021)
13. Zeng, X., Fhager, A., He, Z., Persson, M., Linner, P., Zirath, H.: Development of a time domain microwave system for medical diagnostics. IEEE Tran. Instrum. Meas. 63(12), 2931–2939 (2014)
14. Zeng, X., Fhager, A., Persson, M., Zirath, H.: Performance evaluation of a time-domain microwave system for medical diagnostics. IEEE Tran. Instrum. Meas. 68(8), 2880–2889 (2019)
15. Lodro, M., Greedy, S., Fedeli, S.B., et al.: Statistical characterization of wireless MIMO channels in mode-stirred enclosures. arXiv:2102.00351 (2021)
16. Marimuthu, J., Bialkowski, K.S., Abbosh, A.M.: Software-defined radar for medical imaging. IEEE Trans. Microwave Theory Tech. 64(2), 643–652 (2016)
17. Stancombe, A.E., Bialkowski, K.S.: Portable biomedical microwave imaging using software- defined radio. In: 2018 Asia-Pacific Microwave Conference (APMC), pp. 572–574. IEEE, Piscataway, NJ (2018)
18. Meaney, P., Hartov, A., Raynolds, T., et al.: Low cost, high performance, 16-channel microwave measurement system for tomographic applications. Sensors 20(16), 5436 (2020)
19. Zeng, X., Fhager, A., Persson, M., Linner, P., Zirath, H.: Accuracy evaluation of ultrawideband time domain systems for microwave imaging. IEEE Trans. Antennas Propag. 59(11), 4279–4285 (2011)
20. Meaney, P., Hartov, A., Bulumulla, S., et al.: A 4-channel, vector network analyzer microwave imaging prototype based on software defined radio technology. Rev. Sci. Instrum. 90(4), 044708 (2019)
21. National Instruments: USRP-2901 USRP Software Defined Radio Device. ni.com. https://www.ni.com/sv-se/support/model.usrp-2901.html (2022). Accessed 28 July 2022
22. National Instruments: Decimation (Digital Filter Design Toolkit). ni.com. https://www.ni.com/docs/en-US/bundle/labview-digital-filter-design-toolkit-api-ref/page/lvdfdtconcepts/dfd-decimation.html (2022). Accessed 28 July 2022
23. Analog Devices: RF Agile Transceiver AD9361 (Data Sheet). https://www.analog.com/media/en/technical-documentation/data-sheets/AD9361.pdf (2022). Accessed 30 July 2022
24. Kwon, S., Lee, S.: Recent advances in microwave imaging for breast cancer detection. Int. J. Biomed. Imaging 2016, 5054912 (2016)

How to cite this article: Zeng, X., Orozco, L.G.: Measurement quality of a software defined radio system for medical diagnostics. J. Eng. 1–11 (2022). https://doi.org/10.1049/tje2.12196